Microfluidic device generating stable concentration gradients for long term cell culture: application to Wnt3a regulation of β-catenin signaling†

Elisa Cimetta,[ab] Christopher Cannizzaro,[c] Richard James,[d] Travis Biechele,[d] Randall T. Moon,[d] Nicola Elvassore*[ae] and Gordana Vunjak-Novakovic*[b]

Received 17th May 2010, Accepted 13th September 2010
DOI: 10.1039/c0lc00033g

In developing tissues, proteins and signaling molecules present themselves in the form of concentration gradients, which determine the fate specification and behavior of the sensing cells. To mimic these conditions *in vitro*, we developed a microfluidic device designed to generate stable concentration gradients at low hydrodynamic shear and allowing long term culture of adhering cells. The gradient forms in a culture space between two parallel laminar flow streams of culture medium at two different concentrations of a given morphogen. The exact algorithm for defining the concentration gradients was established with the aid of mathematical modeling of flow and mass transport. Wnt3a regulation of β-catenin signaling was chosen as a case study. The highly conserved Wnt-activated β-catenin pathway plays major roles in embryonic development, stem cell proliferation and differentiation. Wnt3a stimulates the activity of β-catenin pathway, leading to translocation of β-catenin to the nucleus where it activates a series of target genes. We cultured A375 cells stably expressing a Wnt/β-catenin reporter driving the expression of Venus, pBARVS, inside the microfluidic device. The extent to which the β-catenin pathway was activated in response to a gradient of Wnt3a was assessed in real time using the BARVS reporter gene. On a single cell level, the β-catenin signaling was proportionate to the concentration gradient of Wnt3a; we thus propose that the modulation of Wnt3a gradients in real time can provide new insights into the dynamics of β-catenin pathway, under conditions that replicate some aspects of the actual cell-tissue milieu. Our device thus offers a highly controllable platform for exploring the effects of concentration gradients on cultured cells.

Introduction

Microfluidic devices offer the possibility of generating complex and well defined patterns of molecular stimulation, *via* tight control of fluid dynamics on a cell level scale.[1] Recent literature reflects increasing interest in interfacing microfluidic devices with biological systems.[1–11] Examples of highly meritorious gradient makers that are based on microfluidic devices include combined microfluidic and photopolymerization systems for the formation of graded hydrogels,[16] microfluidic devices with substrate-bound molecules,[13] microfluidic systems for the formation of concentration gradients by controlled diffusion[17] or a balance of diffusion and convection,[18] microfluidic mixers,[17] and the membrane-based diffusion chips.[12–14]

Because of the laminar regime that is inherent to fluid flow in micro-channels, the geometry of the microdevice and the flow rates can be tuned to subject the cultured cells to well-defined, diffusion-independent concentration profiles. However, the use of existing microfluidic gradient generators is generally associated with hydrodynamic shear stresses that arise from the small characteristic dimensions of microfluidic channels.[7,15] For most cultured cells, the maintenance of low levels of hydrodynamic shear is vital for the preservation of their well-being.[8,16]

To this end, we designed a microbioreactor that maintains stable and well defined concentration gradients with low hydrodynamic shear, allowing long term cell culture.We then focused our attention on the effects of Wnt3a concentration gradients on cell populations. Wnt proteins are a family of powerful macromolecules involved in a multitude of biological phenomena ranging from early-stage cell fate specification, to embryonic development, cell proliferation, differentiation and tumorigenesis.[17–21] Numerous studies have explored the role of Wnt in cell signaling.[22–26] Of particular interest is the pattern by which the Wnt signals are presented to the cells, through long and short range concentration gradients.[27,28] Still, surprisingly little is known about the effects of Wnt gradients on cell populations and the quantitative data have not yet been reported.

We were interested in studying β-catenin signaling in response to a concentration gradient of Wnt3a, using A375 cells stably expressing pBARVS[29] as a model system. In this model, activation of the BARVS reporter gene could be monitored through the expression of Venus signal. By virtue of its simple design,

[a]*Department of Chemical Engineering, University of Padua, Via Marzolo, 9, I-35131 Padua, Italy. E-mail: nicola.elvassore@unipd.it; Fax: +39 (049) 827-5461; Tel: +39 (049) 827-5469*
[b]*Columbia University, Department of Biomedical Engineering, Vanderbilt Clinic, VC12-234, 622 West 168th Street, New York, NY, 10032. E-mail: gv2131@columbia.edu; Fax: +1 (212) 305-4692; Tel: +1 (212) 305-2304*
[c]*Massachusetts Institute of Technology Harvard-MIT Division for Health Sciences and Technology, Cambridge, MA*
[d]*University of Washington School of Medicine, HHMI and Dept. of Pharmacology, Seattle, WA*
[e]*Venetian Institute of Molecular Medicine, Padova, Italy*
† Electronic supplementary information (ESI) available: Fig. S1–S4. See DOI: 10.1039/c0lc00033g

shear-protective cell culture environment and stable operation, this microbioreactor allowed prolonged culture of A375 cells that was necessary to cover the time span required for gene activation.

Methods

Microfluidic bioreactor design, fabrication and assembly

The hydrodynamic shear stress was calculated for each fluid flow rate as in our previous studies.[16] The level of shear that A375 cells could tolerate in long term experiments (>24 h) was empirically determined at <1 dyne cm^{-2}. For cells cultured in single microfluidic channels at a range of medium flow rates, the fraction of detaching cells was calculated and the shear stress threshold was defined as the value at which 50% of the initial cells detached. The following experiments were conducted at flow velocities corresponding to the hydrodynamic shear below the measured threshold value.

The microfluidic bioreactor was designed to generate stable concentration gradients in long term culture, at low hydrodynamic shear. The device consisted of three 500 μm wide channels aligned in parallel, where the middle channel, 20 mm long, served as the cell culture space (Fig. 1). The channels were connected by an array of smaller perpendicular channels (25 μm wide × 50 μm deep, spaced at 50 μm) that enabled diffusion of molecular species without significant convective flux. This configuration allowed us to obtain sharp and stable concentration gradients inside the middle channel, by diffusional transport between the two outer channels.

The single-layer microfluidic bioreactor was replica-molded in poly(dimethylsiloxane) (PDMS)[30] from a SU-8 mold fabricated through standard lithographic techniques[31] and irreversibly bonded to a 75 × 50 mm microscope slide *via* air plasma treatment, after punching the inlet and outlets ports. The assembled microbioreactor, its tubing and connections were steam sterilized (20 min at 121 °C).

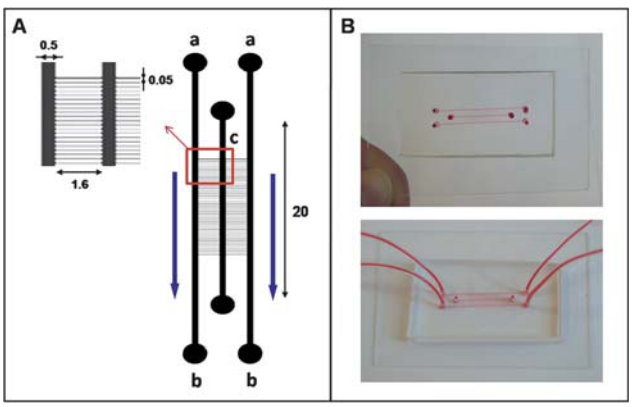

Fig. 1 Microfluidic device. The microfluidic bioreactor (A) was composed of two flow channels with inlets (a) and outlets (b) that flank the cell culture channel (c). Arrows show the flow direction. All dimensions are in mm; the height of the microbioreactor is 50 μm. Panel B shows the top views of the microbioreactor in which the fluidic channels are filled with a dye tracer. The inlet and outlet tubing connects the assembled device to the syringe pump.

Culture of A375 cells stably expressing pBARVS

pBARVS contains 12 TCF/LEF DNA binding elements upstream of a minimal promoter, minP, and drives the Wnt/β-catenin-dependent expression of Venus.[32] It also contains a PGK promoter that drives the constitutive expression of a puromycin resistance cassette for stable selection. These elements were provided by a third generation lentiviral expression system.[33] Lentivirus containing pBARVS was generated and used to infect A375 melanoma cells.[29]

Three days post infection cells were cultured in culture medium containing 2 μg mL^{-1} puromycin. The resulting stable heterogeneous line was then cultured in an EC50 dose of Wnt3a conditioned medium, that was prepared as described in Willert *et al.*[34] 24 h following Wnt3A stimulation, cells were sorted by fluorescence activated cell sorting (FACS) and a narrow gate (1% of the Venus positive cells) of high Venus expressing cells were collected. Sorted cells were cultured for 4 days in culture media without Wnt3a conditioned media to allow Venus expression to return to a low basal expression level. Cells were then sorted by FACS for a narrow gate of the cells expressing the lowest levels of Venus. Cells were then expanded in standard culture flasks in culture medium without Wnt3a (DMEM supplemented with 10% fetal bovine serum, FBS, 1% penicillin-streptomycin) and passaged every 2 days. In order to avoid potential batch-to-batch variability in gradient experiments, Wnt3a conditioned medium was tested and "calibrated". To this end, cells were seeded in 96-well plates at a density of 600 cells mm^{-2} ($n = 5$ per group and time point) and cultured at different dilutions of Wnt3a conditioned medium, from 1% to 100%. At defined time points, the activation of the β-catenin pathway was evaluated by quantifying the fraction of total cells expressing Venus, for each Wnt3a concentration. This "calibration" guided the selection of conditioned medium dilutions for experiments.

Cell seeding and microfluidic bioreactor culture

The culture channel (total volume 0.5 mm^3) was coated with 100 μg mL^{-1} fibronectin for 20 min prior to cell seeding. After removing the fibronectin solution, the entire microfluidic device was filled with culture medium. The lateral channels were sealed with PDMS plugs while the culture channel inlet and outlet were left open. Confluent flasks of A375 cells were enzymatically detached using 0.05% trypsin/EDTA (Sigma-Aldrich), pelleted by centrifugation for 4 min at 1200 rpm and counted. A single-cell suspension at a density of 10^6 cells mL^{-1} in standard culture medium was prepared, and an aliquot of 2 μL was loaded into the culture channel. Attention was paid to avoid placing cells into the small lateral channels (see Fig. S1†). The open/sealed configuration of channels was reversed by opening the lateral flow channels and sealing the inlet and outlet of the culture channel using PDMS plugs. Cells were allowed to adhere for 24 h before starting medium perfusion. After 24 h, the two inlet ports of the side flow channels of each microbioreactor were connected *via* Tygon tubing (0.8 mm ID, 2.4 mm OD, Cole Palmer) to syringes containing standard and conditioned (Wnt3a-containing) medium.

The flow rate, controlled by a digital syringe pump (PHD, Harvard Apparatus), was set at 1 μL min^{-1} per channel. The flow direction was the same for both channels of an individual

microbioreactor, and 5 microbioreactor were operated in parallel. Perfusion was maintained for 12 h, and the cultured cells were analyzed to evaluate fluorescence levels. Two sets of controls were: (*i*) Wnt3a conditioned medium at the dilution used in the perfusion experiment, and (*ii*) perfusion culture in which the microbioreactor was operated with Wnt3a conditioned medium from both flow channels.

Mathematical modeling of flow and transport

The flow regimes and concentration profiles within the microbioreactor were modeled using (*i*) Navier–Stokes equations for incompressible flow modified for the surface forces related component, and (*ii*) the convection-diffusion equation. The equations were solved numerically, for parameters listed in Table 1, using a finite element analysis solver (Comsol Multiphysics). Simulations were performed for different combinations of diffusion coefficients and flow rates listed in Table 1.

To validate the model predictions, the resulting Wnt3a concentration profiles were compared with experimentally measured profiles of fluorescently labeled dextrans: Cascade Blue-conjugate (10 KDa), fluorescein-conjugate (40 KDa), and tetramethylrhodamine-conjugate (70 KDa) (all from Molecular Probes). The calculated diffusion coefficients for each molecule (Table 1) are consistent with literature values.[35] Of note, the Wnt3a molecule could be represented with good approximation by the 40 KDa dextran.

Solutions of each dextran in culture medium were prepared at the final concentration of 1 mg mL^{-1} and supplied to one of the two flow channels. Culture medium alone was used for the second channel. The microbioreactor was assembled as described above, the syringes were loaded with fluids (standard culture medium and culture medium with dissolved fluorescent dextrans), the tubing was connected, and the system was operated at the set flow rate.

The microbioreactor assembly was kept under the microscope (Leica CTR6000) in an environmental chamber (37 °C, 5% CO_2, humidified). Fluorescence images were taken at different time points to assess the stability of the formed gradient and verify the shape of the gradient along the culture channel. This experimental validation was performed at all flow rates listed in Table 1, using three different dextrans. The curves obtained quantifying the fluorescence intensities (ImageJ software), were systematically compared with the modeled concentration profiles.

Quantitative fluorescent imaging of Venus expression in cultured cells

Cell response to Wnt3a concentration gradients were assessed in live cell cultures by measuring the presence and distribution of the fluorescent signal resulting from activation of the targeted Venus-tagged reporter gene. Live cells were incubated with Hoechst nuclear dye (1.5 μg mL^{-1} for 10 min at 37 °C). Cell viability was not affected (as evidenced by Live&Dead® assay, data not shown). Fluorescent images of the nuclei were used to determine the total cell number. The fraction of cells expressing Venus signal was determined by the pair to pair comparisons of fluorescent images of the two channels: Venus in green, and Hoechst in blue, using a script that we developed and that was run using Matlab.

Table 1 Parameters and variables used for the model

Variable	Values	Units	Reference
D_{Wnt3a}	6.00E-11	$m^2\ s^{-1}$	Calculated
D_{10KDa}	4.00E-11	$m^2\ s^{-1}$	Calculated
D_{40KDa}	6.00E-11	$m^2\ s^{-1}$	Calculated
D_{70KDa}	5.00E-10	$m^2\ s^{-1}$	Calculated
μ	0.0007	Pa s	26
ρ	990	$Kg\ m^{-3}$	26
Q	0.17E-11, 0.17E-10, 0.83E-10	$m^3\ s^{-1}$	This study

Results

Establishment of concentration gradients: effects of flow velocity and diffusion coefficient

The capability of the microbioreactor to generate predictable concentration gradients of large soluble molecules was tested for a range of flow rates (0.1, 1, and 5 μL min^{-1}, corresponding to linear velocities inside the flow channels of 6.67×10^1, 6.67×10^2, and 3.33×10^3 μm s^{-1}, respectively), and diffusion coefficients (4×10^{-11}, 6×10^{-11}, and 5×10^{-10} $m^2\ s^{-1}$, corresponding to the molecular weights of chemical species of 10, 40, and 70 KDa respectively). To validate the model predictions and to assess if potential fluctuations in the flow rates may lead to deformations of the gradients shape,[36] concentration gradients developed in the culture channel of the microfluidic bioreactor were experimentally measured for the same values of flow velocity and diffusion coefficient, by using solutions of fluorescently labeled dextrans.

Fig. 2 shows representative results of mathematical modeling (upper panel) and experimental validation (bottom panel). For clarity, only the middle culture channel is shown. Fluorescence images were taken as indicated by the squares in the culture channel schematics on the left.

The effects of flow rate were analyzed at the diffusion coefficient of 6×10^{-11} $m^2\ s^{-1}$, that corresponds to the molecular size of Wnt3a (Fig. 2, top). The color coded bar at the left translates the colors into concentration values of the molecule of interest in the channel expressed as the percent of maximum concentration. The model predicted molecular diffusion as the dominating transport mode at the lowest flow rate of 0.1 μL min^{-1} (corresponding to a linear velocity of 6.67×10^1 and 2.59×10^1 μm s^{-1} in the lateral channel and culture channel, respectively), leading to fast dissipation of the concentration gradient along the length of the microfluidic channel (Fig. 2A).

An increase in flow rate to 1 μL min^{-1} (linear velocity of 6.67×10^2 and 2.59×10^2 μm s^{-1} in the lateral and culture channels, respectively) and 5 μL min^{-1} (linear velocity of 3.33×10^3 and 7.78×10^2 μm s^{-1} in the lateral and culture channels, respectively) resulted in a step-wise concentration gradient that was maintained along the channel length (Fig. 2B and C).

The effects of molecular size of diffusing molecular species were analyzed at the flow rate of 1 μL min^{-1}. For small, fast-diffusing molecules ($D = 5 \times 10^{-10}$ $m^2\ s^{-1}$, 10), there was a dissipation of the gradient along the length of the microfluidic channel, such that a relatively uniform concentration was established in the downstream section of the channel (Fig. 2D). With an increase in molecular size to 40 KDa and 70 KDa (*i.e.*, decrease in the diffusion coefficient to 6×10^{-11} $m^2\ s^{-1}$ and 4×10^{-11} $m^2\ s^{-1}$, respectively), a stable concentration gradient (covering an area from the top to

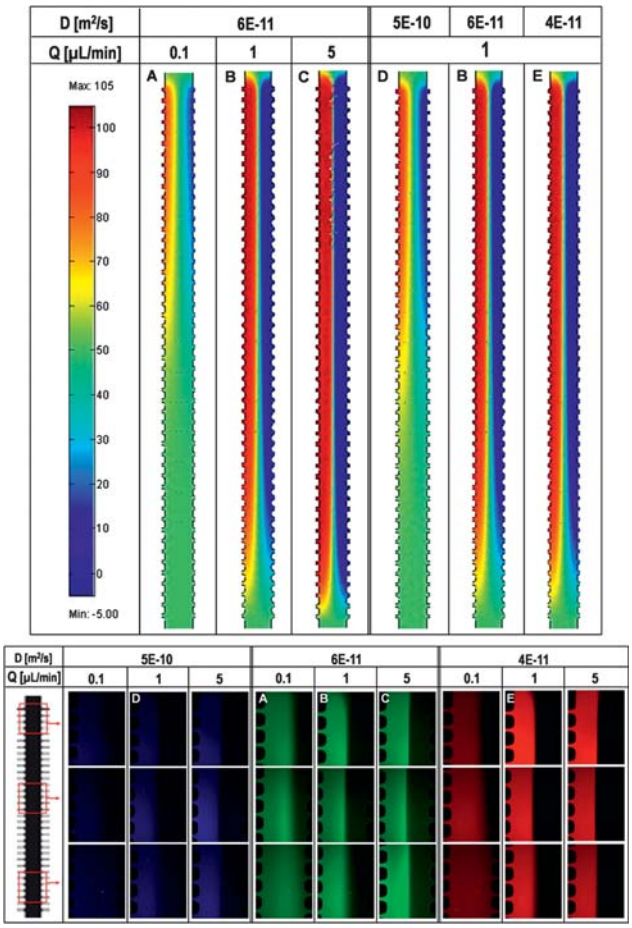

Fig. 2 Experimental validation of the theoretically predicted Wnt3a gradients. Upper panel: theoretically predicted Wnt3a gradients in the microfluidic device. Mathematical modeling allowed visualization of the concentration gradient and spatial distribution of Wnt3a in culture medium (as indicated by the color coded scale at the left). Three different diffusion coefficients and three different flow rates were analyzed as indicated (panels A–E). **Lower panel**: experimentally measured concentration gradients using tracer molecules (fluorescent dextrans with defined molecular weights and diffusion coefficients). The combinations of the flow rates and tracer molecules used for the simulations were experimentally replicated, as indicated by capital letters (A–E).

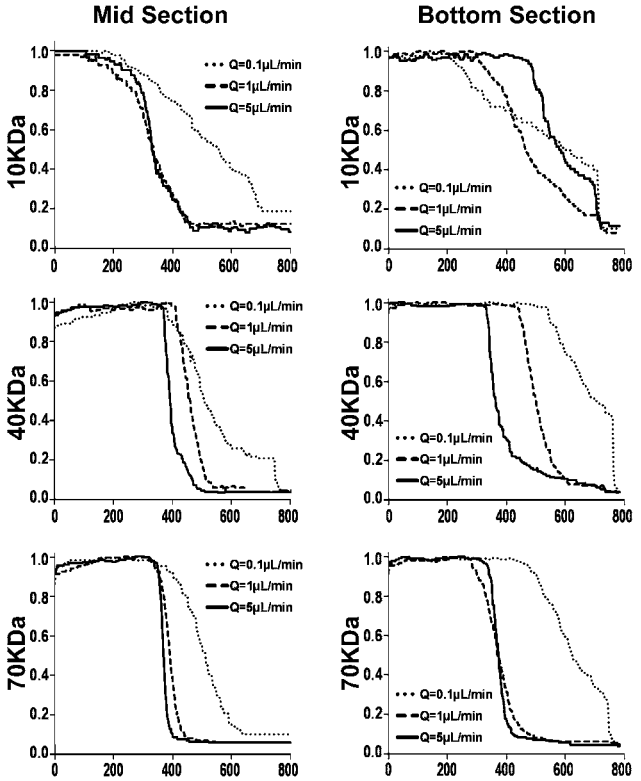

Fig. 3 Fluorescence levels in the mid and bottom sections of the culture channel. The traces correspond to dimensionless values of the fluorescence levels evaluated using ImageJ software. Each graph presents data obtained for one individual molecular weight (10, 40 and 70 KDa respectively) and three different flow rates (0.1, 1 and 5 µL min^{-1}).

the bottom part of the culture channel) was maintained along the channel length, as was the case for relatively high flow rates (Fig. 2B and E). The measured intensity of fluorescence was proportional concentration of the tracer molecule.

To validate the model predictions, we performed quantitative image analysis of the fluorescence intensity across the width of the culture channel, and obtained dimensionless concentration profiles for three molecular species and three perfusion flow rates (Fig. 3).

The experimental and model-predicted concentration profiles confirmed that for low flow rates and low molecular size species molecular diffusion became the dominating transport regime, and that these conditions led to dissipation of the concentration gradient. These data demonstrated that flow rates as low as 1 µL min^{-1} were sufficient for obtaining sharp and stable concentration gradients along the entire culture channel length for diffusing species with molecular size of ≥40 KDa.

In addition, in these experiments and by mathematical modeling, we did not observe changes in the gradient shape due to operator-independent fluctuations in the flow rates.

We verified by further mathematical modeling that the presence of adhering cells did not significantly affect the shape of the concentration gradient within the culture channel (see Fig. S2†). To this end, we simulated the behavior of the microbioreactor under three different conditions: (1) absence of the surface forces, (2) presence of the surface forces, and absence of adhering cells (as in the original manuscript), and (3) presence of both the surface forces and a 20 µm high layer of cells (which is an overestimation) adhering to the bottom of the channel.

Analysis of the gradients in Wnt3a concentration, flow velocity and hydrodynamic shear in the microfluidic device

Based on the experimental validation of modeling data (Fig. 2), the flow rate for establishing a gradient of Wnt3a (diffusion coefficient of 6×10^{-11} m^2 s^{-1}) was set to 1 µL min^{-1}. At this flow rate, the gradients of concentration, velocity and hydrodynamic shear were analyzed in more depth.

Fig. 4 shows mathematical analysis of (*i*) concentration gradients, (*ii*) velocity profiles, and (*iii*) hydrodynamic shear stress for the microfluidic device operating with Wnt3a as the diffusing molecule at a flow rate of 1 µL min^{-1}. Panel A shows the color-coded Wnt3a concentration gradient inside the culture channel, where labels **a**–**d** refer to the sections in which further analyses were carried out.

Panel B, upper graph, shows the modeled plug-flow velocity profiles in the chosen cross sections, and the corresponding normalized values of Wnt3a concentration profiles. **Panel C** summarizes the calculated maximum and minimum values for the velocity and shear stress in sections **a–d** of the culture channel.

Therefore, the system was able to generate predictable and stable concentration gradients with flat and uniform velocity profiles within the culture channel, while exposing the adhering cells to very low values of flow velocity ($2.63 \times 10^{-4} \pm 8.74 \times 10^{-5}$ m s^{-1}) and hydrodynamic shear stress ($2.53 \times 10^{-1} \pm 8.39 \times 10^{-2}$ dyne cm^{-2}). These levels of hydrodynamic shear are at the low end of the hydrodynamic shear levels reported for other microfluidic devices: 0.001–21 dyne cm^{-2} (data from 18 different reports).[19,20]

Activation of the canonical β-catenin pathway in response to constant levels of Wnt3a

To investigate the activation of the β-catenin pathway in response to a range of Wnt3a concentrations, A375 BARVS cells were cultured statically at different constant concentrations of Wnt3a, obtained by diluting Wnt3a conditioned medium (at 1–100%). The activation of β-catenin pathway in cultured cells was proportionate to the concentration of Wnt3a, as evidenced by the percentage of Venus-expressing cells. The Venus signal was detected a few hours after Wnt3a addition, and increased with time of culture (data not shown). The fraction of cells expressing Venus signal was determined as the ratio between the number of fluorescent cells and the number of total cells in each observation field. Quantitative image analysis showed that an increase in the concentration of ligand resulted in an increase in the number of Venus positive cells (Fig. S3†). Of note, the number of Venus-expressing cells appeared to not significantly increase above a certain Wnt3a concentration (which was batch-dependent but mostly ranged between 25 to 50%). Based on these results, the range of dilutions of the Wnt3a conditioned medium to be used in microfluidics experiments was set to the sub-threshold values in the range of 1–50%.

Differential activation of the canonical β-catenin pathway in response to a gradient of Wnt3a

To investigate differential activation of the β-catenin pathway, A375 BARVS cells were cultured for up to 2 days in the microfluidic device, subjected to flow-generated Wnt3a concentration gradients. Cells subjected to a constant concentration of Wnt3a were used as controls. The microfluidic gradient was readily established by perfusing Wnt3a conditioned medium through one lateral channel, and plain medium through the other lateral channel. Constant concentration of Wnt3a was established by perfusing Wnt3a medium through both channels. Fig. 5A shows representative bright field and fluorescent images of cells cultured at constant Wnt3a concentrations (upper row) and under a gradient of Wnt3a concentration (bottom row).

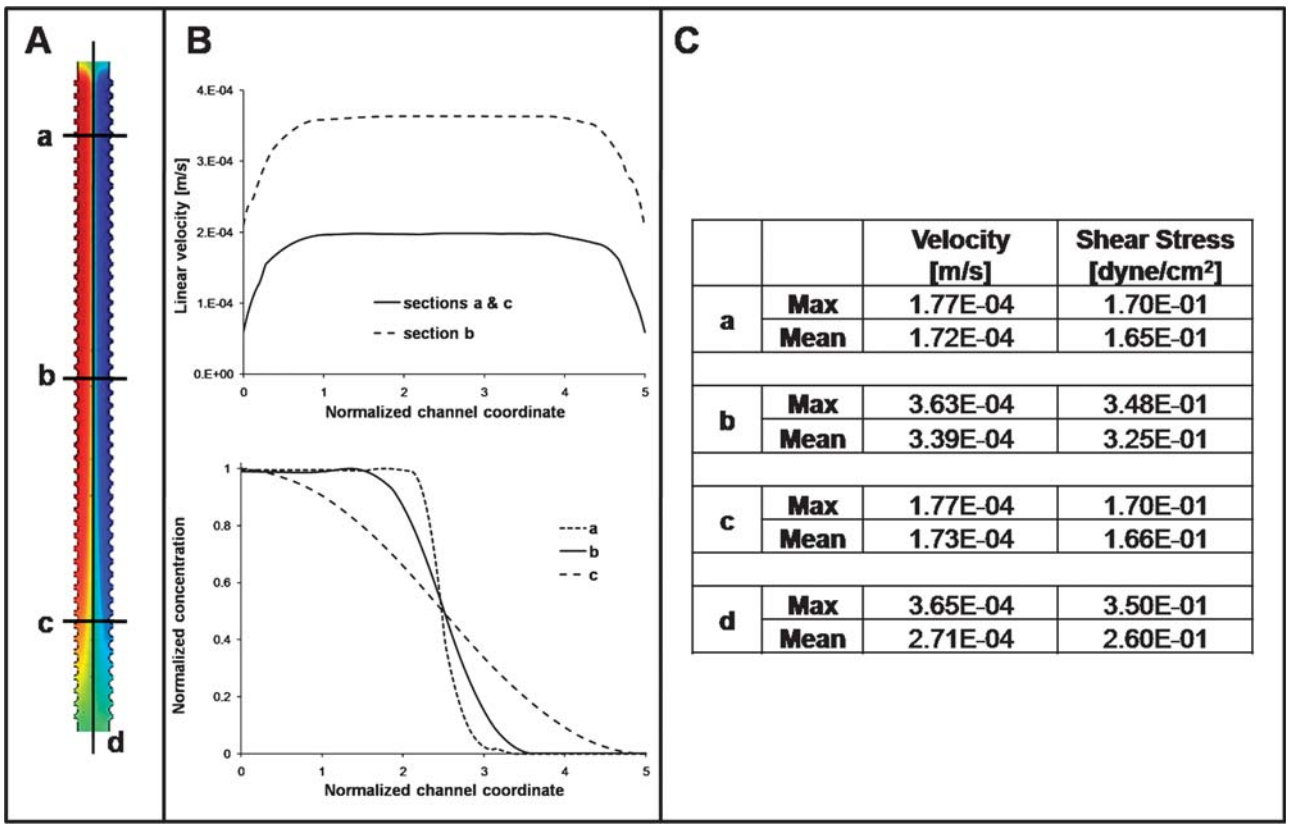

		Velocity [m/s]	Shear Stress [dyne/cm²]
a	Max	1.77E-04	1.70E-01
	Mean	1.72E-04	1.65E-01
b	Max	3.63E-04	3.48E-01
	Mean	3.39E-04	3.25E-01
c	Max	1.77E-04	1.70E-01
	Mean	1.73E-04	1.66E-01
d	Max	3.65E-04	3.50E-01
	Mean	2.71E-04	2.60E-01

Fig. 4 Gradients of concentration, velocity, and shear stress in the cell culture channel. Panel A: the flow characteristics of four different sections of the culture channel (a, b, c, d) were modeled for the Wnt3a diffusion coefficient of 6×10^{-11} m^2 s^{-1} and the flow rate of 1 μL min^{-1}. **Panel B**: plug-like velocity profiles in cross sections a, b and c (upper graph), and the corresponding concentration profiles (bottom graph). **Panel C**: the maximum and average values for the flow velocity and shear stress in all four sections of the culture channel.

Cells from the control experiments showed uniform expression of Venus throughout the entire population. In contrast, in the microfluidic Wnt3a gradient experiments, Venus expression was observed only in cells adjacent to the source of the Wnt3a ligand. Quantitative results obtained by image processing of 20 sections per condition are shown in Fig. 5B. Each section, (2 mm long region of the 500 μm wide cell culture channel) located in the mid section of the 20 mm long culture channel, was divided into three regions perpendicular to the direction of Wnt3a gradient (labeled "left", "middle" and "right", and the Wnt3a concentration decreases from left to right).

The microfluidics-generated Wnt3a gradient elicited a proportionate response of the Venus signal with the highest expression in the region of highest Wnt3a concentration ("left"), practically no expression in the region of lowest Wnt3a concentration ("right"), and a graded response in the transient region ("middle"). Specifically, the fraction of cells expressing Venus signal at left third of the channel was 9 fold higher than that on cells on the right third of the channel.

Statistically significant differences in the fraction of cells expressing Venus were detected between each pair of channel sections for Wnt3a gradient conditions, but not for controls with uniform Wnt3a concentration (Fig. 5B).

Interestingly, the exposure of cells to the gradient of Wnt under microfluidic culture conditions decreased the number of Venus positive cells, to 0.6–0.7 of the corresponding levels measured in the static (microwell) controls. However, the internal ratios of the numbers of Venus positive cells at different concentrations remained the same in the two systems. These quantitative data proved the effective differential activation of the cells in response to the gradients of Wnt3a concentration generated by medium flow in the microfluidic device. Additional analyses demonstrated that differences in fluorescence expression of cells (and thus the activation of the Wnt3a pathway) arose along the length of the culture channel according to the imposed concentration gradient (see Fig. S3 and S4†).

As the cells used in the experiment are polyclonal with respect to the reporter, cell to cell variations in intensity of the fluorescent signal were not evaluated.

Discussion and conclusions

Our goal was to design a microbioreactor capable of generating well characterized concentration gradients over an adhering cell population (within a 500 μm wide culture channel) under conditions of low shear stress (Fig. 1). We investigated the capability for presenting spatially and temporally stable concentration gradients to cultured cells by mathematical modeling of flow and mass transport, to obtain maps of concentrations in the culture channel, for different flow velocities and molecular sizes of diffusing species. The model predictions were validated in experimental studies that utilized fluorescent molecular tracers (Fig. 2 and 3).

Mathematical modeling allowed precise quantitation of the spatial-temporal evolution of concentration profiles as a function of the microfluidic configuration, medium flow rate and the diffusion coefficient of molecular species (Fig. 4). The natural tendency of a concentration gradient to dissipate could also be described. For example, an axial gradient could be generated only if the characteristic dissipation time ($\tau_D = w^2/D$; where w is the cell culture channel width and D is the diffusion coefficient) was comparable to the fluid culture-chamber residence time ($\tau p = V/Q$; where V and Q are the volume and the flow rate within the cell

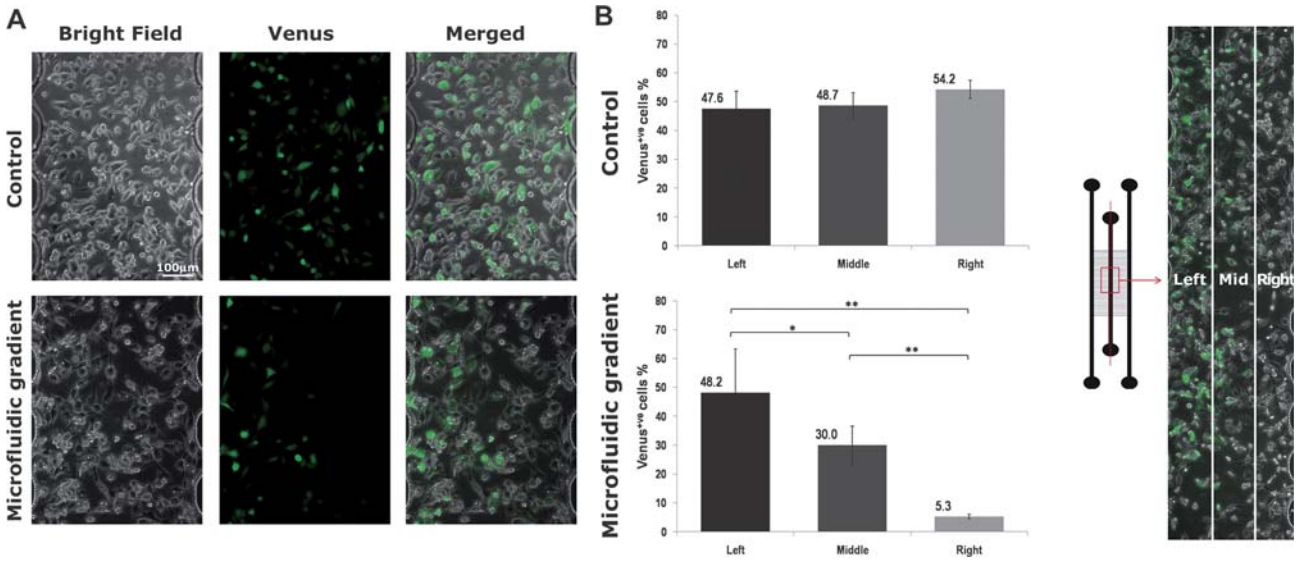

Fig. 5 Case study: activation of the canonical Wnt3a/β-catenin pathway in cells cultured in microbioreactors. Panel A: cells were exposed for 12 h either to uniform Wnt3a concentration (control, top row) or to a microfluidic-generated gradient of Wnt3a concentration (microfluidic gradient, bottom row). Bright field images (left column), fluorescent images of the activated Venus-expressing cells (middle column) and merged images of Venus and bright field (right column) are shown. Images were taken in the mid sections of the culture channel. **Panel B**: fraction of total cells expressing Venus in control cells exposed to a constant concentration of Wnt3a (upper histogram) and in cells exposed for 12 h to a microfluidic-generated gradient of Wnt3a (lower histogram). Data refer to cell numbers measured in three regions of a 2 mm long section of the cell culture channel that were oriented perpendicular to the direction of Wnt3a gradient ("left", "middle" and "right", the Wnt3a concentration decreasing from left to right). Each image is a merge of the fluorescent Venus signal and the corresponding bright field. The numbers refer to the ratio between the number of Venus-expressing cells and the total number of cells. Images were taken in the mid sections of the culture channels (* $p < 0.05$. ** $p < 0.001$).

culture channel, respectively). These studies allowed us to select fluid flow rates suitable for establishing stable concentration gradients of a range of molecular species (10–70 KDa, where 40 KDa corresponds to the Wnt3a). In each case, the concentration gradient could be established by simply adjusting the flow rate according to the species' diffusion coefficient (Fig. 2 and 3).

The microfluidic configuration proposed here provided hydrodynamic shear stresses acting at the cultured cells that were substantially lower than in existing devices.[2,5] Still, we could identify, both experimentally and *via* computational simulation, the presence of small velocity fields along the axis of the culture channel. Since velocity gradients determine the shear stress, a proper design of the microfluidic configuration and the operating parameters is critic for avoiding negative effects of shear stress on cell culture.

The microbioreactor allowed prolonged culture of cells under static and perfused conditions, with perfusion enabling the maintenance of either constant concentrations or gradients of soluble diffusing species.

As a case study, we investigated whether a gradient in Wnt3a concentration in culture medium initiated a proportionate transcriptional response of a Wnt/β-catenin reporter in cultured cells. Under the conditions of medium perfusion that generated a spatial gradient of Wnt3a over the cell culture field, the expression of Wnt reporter along the longitudinal axis of the microbioreactor followed a steep sigmoid-like pattern.

Overall, the relative changes in the fractions of Venus expressing cells from one concentration to another were comparable for the 96-well plates and microbioreactor cultures (Fig. 5). However, the concentration gradient over a large population of cells is more representative of the actual gradients regulating cell fate and function in developing tissues.

Gradients of diffusible Wnt ligands have been postulated to regulate several *in vivo* cellular responses including target gene transcription,[37,38] polarity[39,40] and directed migration.[40] Until recently there have been few techniques capable of testing the hypothesis that gradients of Wnt signaling are sufficient to direct the above described cellular responses. The most significant hurdle that has faced researchers who wish to test the effects of *in vitro* gradients of soluble molecules on cellular responses is the inability to maintain the shape of the gradient over extended periods of time. The reason for this difficulty in establishing steady-state gradients of soluble molecules lies in the fact that diffusion of the molecules over time causes the shape of the gradient to change. The device presented in this manuscript is one of the first that will allow for long-term investigation of morphogen gradient dependent responses (Fig. 5), and will be important for future investigation of cellular responses to signaling events in a variety of exciting contexts including cell migration, differentiation of embryonic stem cells, and gradient-dependent transcriptional responses.

These results, applied to the developmentally relevant family of Wnt3a molecules, are promising for further exploring the roles of concentration gradients on cell populations.

Acknowledgements

We gratefully acknowledge support of the University of Padova and Fondazione CARIPARO (EC), and NIH (2P41-EB002520 to GVN, R01 GM073887 toRTM), and HHMI (RTM).

References

1 T. M. Keenan and A. Folch, *Lab Chip*, 2008, **8**, 34–57.
2 D. Amarie, J. A. Glazier and S. C. Jacobson, *Anal. Chem.*, 2007, **79**, 9471–9477.
3 D. J. Beebe, G. A. Mensing and G. M. Walker, *Annu. Rev. Biomed. Eng.*, 2002, **4**, 261–286.
4 J. A. Burdick, A. Khademhosseini and R. Langer, *Langmuir*, 2004, **20**, 5153–5156.
5 N. L. Jeon, S. K. W. Dertinger, D. T. Chiu, I. S. Choi, A. D. Stroock and G. M. Whitesides, *Langmuir*, 2000, **16**, 8311–8316.
6 T. Kang, J. Han and K. S. Lee, *Lab Chip*, 2008, **8**, 1220–1222.
7 L. Kim, Y.-C. Toh, J. Voldman and H. Yu, *Lab Chip*, 2007, **7**, 681–694.
8 T. H. Park and M. L. Shuler, *Biotechnol. Prog.*, 2003, **19**, 243–253.
9 S. K. Sia and G. M. Whitesides, *Electrophoresis*, 2003, **24**, 3563–3576.
10 T. M. Squires and S. R. Quake, *Rev. Mod. Phys.*, 2005, **77**, 977–1016.
11 G. M. Whitesides, *Nature*, 2006, **442**, 368–373.
12 J. Diao, L. Young, S. Kim, E. A. Fogarty, S. M. Heilman, P. Zhou, M. L. Shuler, M. Wu and M. P. DeLisa, *Lab Chip*, 2006, **6**, 381–388.
13 S. Chung, R. Sudo, P. J. Mack, C. R. Wan, V. Vickerman and R. D. Kamm, *Lab Chip*, 2009, **9**, 269–275.
14 S. Toetsch, P. Olwell, A. Prina-Mello and Y. Volkov, *Integr. Biol.*, 2009, **1**, 170–181.
15 Y. Chisti, *Crit. Rev. Biotechnol.*, 2001, **21**, 67–110.
16 E. Cimetta, E. Figallo, C. Cannizzaro, N. Elvassore and G. Vunjak-Novakovic, *Tissue Engineering: Methods*, 2009, **47**, 81–89.
17 H. Clevers, *Cell*, 2006, **127**, 469–480.
18 C. Y. Logan and R. Nusse, *Annu. Rev. Cell Dev. Biol.*, 2004, **20**, 781–810.
19 R. T. Moon, *Science Signaling*, 2005, **271**, cm1.
20 R. T. Moon, B. Bowerman, M. Boutros and N. Perrimon, *Science*, 2002, **296**, 1644–1646.
21 R. T. Moon, A. D. Kohn, G. V. DeFerrari and A. Kaykas, *Nat. Rev. Genet.*, 2004, **5**, 689–699.
22 A. Otto, C. Schmidt, G. Luke, S. Allen, P. Valase, F. Muntoni, D. Lawrence-Watt and K. Patel, *J. Cell Sci.*, 2007, **121**, 2939–2950.
23 S. Ueno, G. Weidinger, T. Osugi, A. D. Kohn, J. L. Golob, L. Pabon, H. Reinecke, R. T. Moon and C. E. Murry, *Proc. Natl. Acad. Sci. U. S. A.*, 2007, **104**, 9685–9690.
24 S. Maretto, M. Cordenonsi, S. Dupont, P. Braghetta, V. Broccoli, B. Hassan, D. Volpin, G. M. Bressan and S. Piccolo, *Proc.Natl. Acad. Sci. U. S. A.*, 2003, **100**, 3299–3304.
25 J. L. Green, T. Inoue and P. W. Sternberg, *Cell*, 2008, **134**, 646–656.
26 E. S. Witze, E. S. Litman, G. M. Argast, R. T. Moon and N. G. Ahn, *Science*, 2008, **320**, 365–369.
27 K. Bartscherer and M. Boutros, *European Molecular Biology Organization*, 2008, **9**, 977–982.
28 A. Aulehla, W. Wiegraebe, V. Baubet, M. B. Wahl, C. Deng, M. Taketo, M. Lewandoski and O. Pourquié, *Nat. Cell Biol.*, 2008, **10**, 186–193.
29 T. L. Biechele and R. T. Moon, *Methods Mol. Biol.*, 2009, **468**, 99–110.
30 Y. Xia and G. M. Whitesides, *Annu. Rev. Mater. Sci.*, 1998, **28**, 153–184.
31 A. Tourovskaia, X. Figueroa-Masot and A. Folch, *Nat. Protoc.*, 2006, **1**, 1092–1104.
32 A. Rekas, J. R. Alattia, T. Nagai, A. Miyawaki and M. Ikura, *J. Biol. Chem.*, 2002, **277**, 50573–50578.
33 T. Dull, R. Zufferey, M. Kelly, R. J. Mandel, M. Nguyen, D. Trono and L. Naldini, *J. Virol.*, 1998, **72**, 8463–8471.
34 K. Willert, J. D. Brown, E. Danenberg, A. W. Duncan, I. L. Weissman, T. Reya, J. R. Yates and R. Nusse, *Nature*, 2003, **423**, 448–452.
35 J. Braga, J. M. P. Desterro and M. Carmo-Fonseca, *Mol. Biol. Cell*, 2004, **15**, 4749–4760.
36 D. Irimia, G. Charras, N. Agrawal, T. Mitchison and M. Toner, *Lab Chip*, 2007, **7**, 1783–1790.
37 C. J. Neumann and S. M. Cohen, *Development*, 1997, **124**, 871–880.
38 M. Zecca, K. Basler and G. Struhl, *Cell*, 1996, **87**, 833–844.
39 A. Dabdoub and M. W. Kelley, *J. Neurobiol.*, 2005, **64**, 446–457.
40 M. T. Veeman, J. D. Axelrod and R. T. Moon, *Dev. Cell*, 2003, **5**, 367–377.